Turbulent air-sea fluxes in the Gulf of Guinea during the AMMA experiment

Denis Bourras, Alain Weill, Guy Caniaux, Laurence Eymard, Bernard Bourlès, S. Letourneur, D. Legain, Erica Key, François Baudin, B. Piguet, et al.

Turbulent air-sea fluxes in the Gulf of Guinea during the AMMA experiment

D. Bourras,[1] A. Weill,[1] G. Caniaux,[2] L. Eymard,[3] B. Bourlès,[4] S. Letourneur,[5] D. Legain,[2] E. Key,[6] F. Baudin,[5] B. Piguet,[2] O. Traullé,[2] G. Bouhours,[2] B. Sinardet,[7] J. Barrié,[2] J. P. Vinson,[1] F. Boutet,[1] C. Berthod,[5] and Aurélien Clémençon[5]

Received 10 June 2008; revised 1 December 2008; accepted 13 February 2009; published 25 April 2009.

[1] Turbulent fluxes at the air-sea interface were estimated in the framework of the African Monsoon Multidisciplinary Analysis (AMMA) international program. A specific flux measurement mast was designed so as to minimize aerodynamic flow distortion and vibrations. The mast was installed on the research vessel *Atalante* that cruised in the Gulf of Guinea during the onset of the African monsoon, in June–July 2006. Turbulent fluxes were calculated with an eddy covariance method and with a spectral method. Calculation of eddy correlation fluxes required a correction of flow distortion at turbulent scales, which was performed with a new statistical technique. Application of the spectral flux calculation method revealed that an imbalance term was required, in agreement with results from earlier experiments, and indicated that the value of the Kolmogorov constant (0.55) should not be modified. Bulk exchange coefficients calculated are in good agreement with earlier parameterizations in medium wind conditions.

Citation: Bourras, D., et al. (2009), Turbulent air-sea fluxes in the Gulf of Guinea during the AMMA experiment, *J. Geophys. Res.*, *114*, C04014, doi:10.1029/2008JC004951.

1. Introduction

[2] African Monsoon Multidisciplinary Analysis (AMMA) is an international campaign devoted to the study of the West African Monsoon, its origin, its variability, and its influence at different scales on environment. Because of the nature of the knowledge to be developed in the AMMA environment, several disciplines have indeed to cooperate which is one originality of AMMA, see AMMA project [*Redelsperger et al.*, 2006].

[3] One aspect of AMMA was the EGEE campaign, which studied ocean dynamics of the Gulf of Guinea at different spatial and temporal scales. This included the study of oceanic circulation and variability in the upper layers of the Eastern Tropical Atlantic Ocean, focusing on the Gulf of Guinea (GG). Relationships between GG circulation and variability and relationships with climate remain relatively unknown though it is established that monsoon intensity is related to the intensity of Marine Boundary Layer meridional gradients between GG and the African continent. A systematic survey of the region, EGEE [see *Bourlès*, 2003; *Bourlès et al.*, 2007], was conducted in 2002, with follow-on campaigns in 2005, 2006 and 2007 to monitor the oceanic conditions in the Gulf of Guinea during the two extreme phases of the West African Monsoon.

[4] In May–June 2006, an intensive set of observations was collected during the AMMA Special Observing Period for the analysis of air-sea exchanges at the ocean-atmosphere interface. One of the objectives was to determine relevant momentum and heat turbulent fluxes at the air-sea interface, following methods already described by several authors: see *Fairall et al.* [1996, 1997], *Persson et al.* [2005], *Dupuis et al.* [1997], *Edson et al.* [1991, 1998], *Bradley et al.* [1991], *Yelland et al.* [1998], *Taylor and Yelland* [2000], *Large and Pond* [1982], *Champagne et al.* [1977], or *Drennan et al.* [1996], to quote a few. Improved flux measurement methods, such as the inertial dissipation (ID) or the eddy correlation (EC) methods have been developed at Centre d'Etude des Environnements Terrestre et Planétaires (CETP) using data collected since the "Surface de l'Océan Flux et Interactions avec l'Atmosphère/Atlantic Structure Transition Experiment" (SOFIA/ASTEX) in 1992 [*Weill et al.*, 1995]. These methods have been successfully applied during several experiments, as referenced in papers by *Dupuis et al.* [1995, 1997], H. Dupuis et al. (Heat fluxes by the inertial dissipation method during FETCH, paper presented at Symposium on Air-Sea Interface, University of New South Wales, Sydney, New South Wales, Australia, 11–15 January 1999), *Pedreros et al.* [2003], *Dardier et al.* [2003], and *Brut et al.* [2005].

[5] Flux measurement and parameterizations have been analyzed with success and with an excellent precision in the tropical regions using data collected by the "Tropical Ocean and Global Atmosphere–Coupled Ocean-Atmosphere Response Experiment" (TOGA-COARE) [see *Fairall et al.*,

[1]CETP, Vélizy-Villacoublay, France.
[2]GAME, CNRM, Météo-France, Toulouse, France.
[3]LOCEAN, Paris, France.
[4]IRD, Plouzané, France.
[5]DT, INSU, Meudon, France.
[6]RSMAS, University of Miami, Miami, Florida, USA.
[7]Institut Carnot de Bourgogne, Dijon, France.

0148-0227/09/2008JC004951

Figure 1. Overview of the flux measurement system, mounted on R/V *Atalante*.

1997]. However, these methodologies have not been applied to the Gulf of Guinea, particularly during the monsoon, when complex air-sea forcing demands precise, all-encompassing validation data sets. In this context, ''qualified local fluxes'' as in previous experiments are necessary for flux parameterization, to compare with other estimates as with satellite fluxes [*Bourras*, 2006; *Eymard et al.*, 2003] or to be used in models, as in the paper by *Caniaux et al.* [2005].

[6] In this paper, we describe and discuss these different fluxes obtained during more than one month, between 2 June and 5 July 2006. Though the data shown were collected on the same vessel *Atalante* as in the ''Flux, état de la mer, et télédétection en conditions de fetch variable'' (FETCH) [*Hauser et al.*, 2003] experiment, some changes have been made to the flux measurement system, including (1) construction of a new flux platform atop the permanent fixed mast on the bow of the ship (Figure 1); (2) a redundancy in the heat flux measurement system, consisting of both a refractometer [*Delahaye et al.*, 2001] and a Licor 7500 sensor to aid in the estimation of humidity fluctuations; and (3) a new motion package (angular and linear accelerations of the ship) at the level of the flux platform. Figure 2.

[7] First, we describe the experimental setup and present features of the new flux package related to minimizing flow distortion and vibration. Then, flux methodology is discussed, focusing on calculations made with the ID and the EC methods. We use temporal structure function of order three to compute turbulent dissipation rate using *Kolmogorov*'s [1941] -4/5 law, which is analyzed as a complement to the ID method. We also analyze several new arguments showing the relevance of $-0.5\ z\ L^{-1}$ imbalance as proposed by *Dupuis et al.* [1997] during SOFIA-ASTEX and the ''Structures des Echanges Mer-Atmosphère Prospections des Hétérogénéités Océaniques, leur Répartition, projet d'Expérience'' (SEMAPHORE) experiments, which complements those suggested by *Dardier et al.* [2003] during the FETCH experiment. For the EC method, the importance of a good time synchronization of the different variables used to get fluxes is pointed out. Fluxes and bulk exchange coefficients [*Monin and Obukhov*, 1954] derived from the EGEE 2006 data set in the Gulf of Guinea are presented, discussed and compared to the literature, followed by a conclusion.

2. Experimental Setup

[8] An effort to improve the flux instrument package used in the previous campaigns SEMAPHORE, FETCH, ''Couplage avec l'Atmosphère en Conditions Hivernales/Front and Atlantic Storm-Track Experiment'' (CATCH-FASTEX) [*Eymard et al.*, 1999], and EQUALANT [*Brut et al.*, 2005] was initiated in 2004 by scientists and engineers at CETP, Division Technique de l'Institut National des Sciences de l'Univers (DT-INSU), Centre National de Recherches en Météorologie (CNRM), and Laboratoire d'océanographie (LOCEAN). The new system was designed to offer a reduced aerodynamic drag, and to have no eigen vibration modes in the frequency range 0–25 Hz that would affect wind measurements. It was also stressed that the new system should be easily ported to most research vessels and should provide a consistent set of instruments for every campaign, with a constant dimensional spacing between sensors. The system was built especially with EGEE in mind, which was to be conducted on the R/V *Atalante* in May–June 2006. The location of the new system on the *Atalante* was carefully studied, because large distortion effects were expected on a 85-m-long ship.

2.1. EGEE-AMMA and the *Atalante*

[9] During EGEE, the research vessel *Atalante* (Ifremer) transected a region from 10°S 10°W to 5°N 5°E, during the period 25 May 2006 to 5 July 2006. Two three-week legs were completed during the EGEE-AMMA cruise, the first from 25 May to 14 June, during which the *Atalante* visited the southwestern Gulf of Guinea, and the second from 17

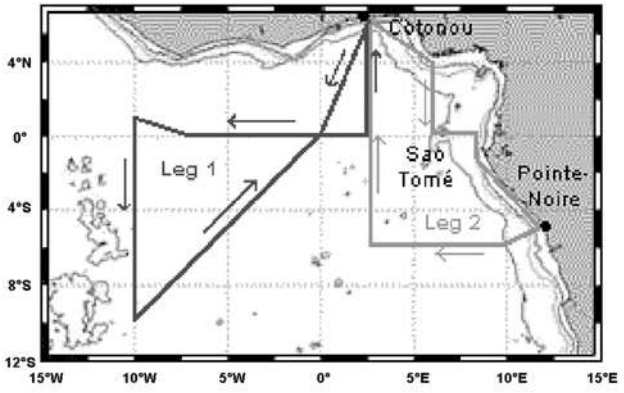

Figure 2. Artist's view of the flux system: instruments description.

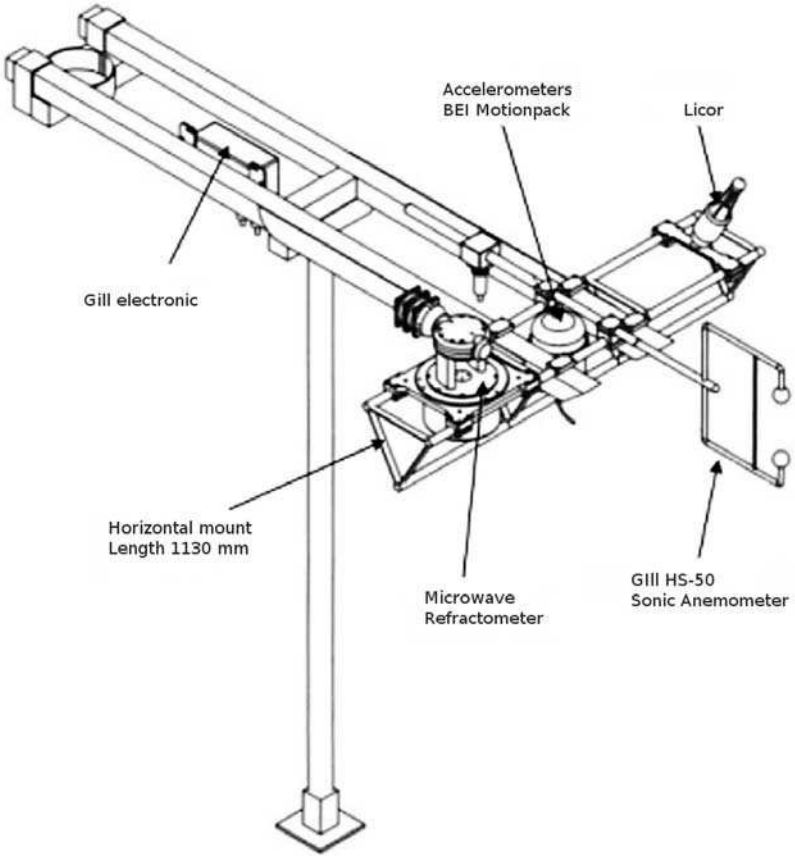

Figure 3. EGEE-AMMA cruise: overview of the two legs.

June to 5 July, as shown in Figure 3. The scientific program was a compromise between the requirements of the numerous science communities present onboard. The manifold science objectives included a repeat sampling of the regional oceanic current systems, as had been conducted in previous EGEE campaigns. The 2006 cruise track also featured a N-S transect to sample the atmospheric structure of the African Monsoon, and several stations for the maintenance and deployment of instrumented moorings for the PIRATA network [*Servain et al.*, 1998; *Bourlès et al.*, 2008]. Air-sea fluxes were calculated along this complex trajectory only when the wind was blowing ±35° relative to the ship bow and when the ship was cruising at 2–3 kn (1 kn = 1.85 km h^{-1}), to maximize accuracy. Because of these strict criteria, much of the flux data collected during the transit and northward radials were unusable. In spite of this, more than 200 h of flux data were collected. It represents more than one third of the time spent at sea. Conditions were mostly calm (5–7 m s^{-1} wind) during the cruise, with large specific humidities (15–20 g kg^{-1}) and sea surface temperatures (SST) in the range 28–30°C. Two specific features of the EGEE cruises were (1) around each PIRATA buoy, specific 6-h flux measurement cruises were performed for fine flux variation analysis and cross validation of measured data and (2) aircraft flux measurement were performed by an ATR 42 along the cruise of the ship during the northward branch of the second leg. Results from these cruises will be described in a future paper.

2.2. Flux Measurement System

[10] Rapidly sampled data (20 to 50 Hz sample rate) required for turbulent flux calculation included the three wind components, humidity, air temperature, and 6 accelerations (3 angular and 3 linear). The flux measurement system used for EGEE is a group of four sensors, namely, an HS-50 Gill three-axis sonic wind anemometer, which provides wind components and sonic air temperature, a Licor LI-7500 humidity fluctuation measurement sensor, a six degrees of freedom accelerometer (BEI motion pack), and a microwave refractometer developed at CETP-DT INSU.

[11] The Licor and the refractometer were used for redundancy, cross-validation of humidity measurements. The microwave refractometer is sensitive to temperature and humidity fluctuations [*Delahaye et al.*, 2001]. For EGEE it was calibrated in two stages. First a slow calibration was performed with respect to Campbell station meteorological measurements. Then, turbulent calibration was performed in terms of spectral variance in relation with turbulent measurements.

[12] Sampling frequencies are 20 Hz for the Licor, 50 Hz for the Gill and the refractometer. Analogue outputs from the BEI were sampled at 50 Hz at the level of the mast, and Licor data were resampled at 50 Hz in order to perform a simultaneous acquisition on a PC, processed with the Labview (trademark) software.

[13] Ancillary data are required for flux calculation with the spectral and bulk methods. They were provided by "slow" (1–10 s) meteorological instruments: Two Gill

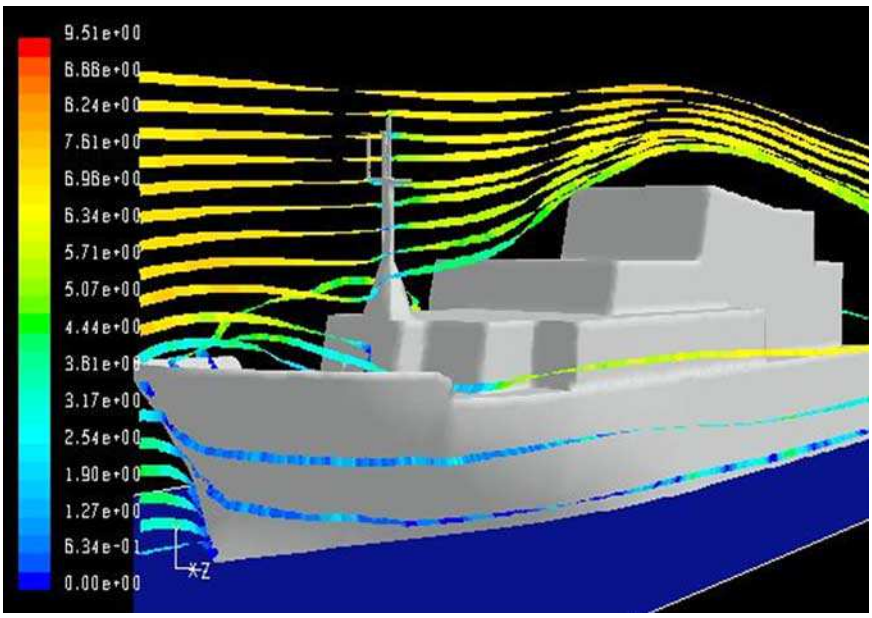

Figure 4. Model of the *Atalante* used for flow distortion simulations. Streamlines are colored as a function of wind speed (7 m s^{-1} at infinite, upwind), and they are twisted as a function of vertical wind angle.

Aspirated Radiation Shield with HMP233 thermo-hygrometers Vaisala (one either side of the mast) as well as two Young Propeller 05106 anemometers. Additional data were provided by two two-plate atmospheric pressure devices, the ship's thermosalinograph (which measures bulk SST at 4 m depth) and an infrared radiometer for radiometric skin SST. Navigation data included three compasses, two GPS, an electromagnetic log and a Doppler log, which are required for the calculation of the true wind (wind with respect to the sea surface or the seafloor). Data intercomparisons were performed to select the most accurate "slow" instruments for further use in flux calculations. For instance, it was found that one of the GPS was less accurate than the other and that one of the Young anemometers had a systematic bias, possibly because of its slightly sheltered position with respect to the incoming wind. The true wind calculation was made with data from the sonic anemometer on the mast, the electromagnetic loch, one GPS, and one compass.

2.3. Flow Distortion Simulations

[14] The motivation for the flow distortion analysis was twofold, namely, to (1) estimate the wind distortion effect for every possible location of the flux system on the *Atalante* and (2) to optimize the aerodynamics of the flux measurement system.

[15] In earlier experiments, the flux system was mounted at the top of a 10 m mast on the ship's bow. This configuration was discarded because sensor maintenance was difficult and dangerous at sea, which could lead to cruises with minimal data return if an instrument was damaged or failed. In addition, the instruments had to be first mounted with the mast lying in a horizontal position for easier access. This put the sensors at risk when the crane then lifted the mast toward its vertical position. The *Atalante* had an existing platform 15 m behind the bow, offering a 1 sq. m working space at 15 m above sea level, accessible with a ladder (Figure 1). A first series of simulations was conducted to check whether it was a reasonable choice to install the flux package on this existing platform. The unknowns were the rather large distance between the platform and the bow and the relevance of the small height of the mast.

[16] The distortion simulation is a very important step to qualify flux measurement, see for example *Yelland et al.* [2002] and *Dupuis et al.* [2003]. For EGEE, it was performed with a commercial code (from fluent Inc.). The simulation was steady, three dimensional, for wind only (momentum and mass time-dependent equations), and used a Reynolds stress turbulence model. The domain of simulation was a rectangular channel of 1000 m in the streamwise dimension, 1000 m crosswise, and 100 m in the vertical. Boundary conditions were symmetric conditions on top, a smooth wall (zero wind) as sea surface, and a prescribed horizontal wind speed of 7 m s^{-1}. To increase realism, part of the flux mast was modeled on the platform expected to receive the instruments (Figure 4). The simulated flow was analyzed in terms of vertical wind angle, horizontal wind angle, and wind intensity. As shown in Figure 5a, wind speed is slightly decreased (-0.2 m s^{-1}) near the instruments (17 m above sea level) if the horizontal wind angle is 0°. In contrast, wind accelerates by up to 1.5 m s^{-1} at 90°, which is large. The azimuth wind angle is itself modified by the body of the ship. It is amplified proportionally to its magnitude, as shown in Figure 5b. For example, if the flow comes onto the ship with a 20° azimuth angle, then the wind angle is ~25° at the level of the instruments. The vertical wind angle varies between 4° and 8° for azimuth wind angles ranging from 0 to 90°, as shown in Figure 5c. Sonic anemometer data plotted on Figure 5c defines an order of magnitude of the vertical wind angle, similar to the angle found with the simulations (5–8°). This range of vertical distortion angle was also recently confirmed with a tank experiment [*Traullé et al.*, 2008].

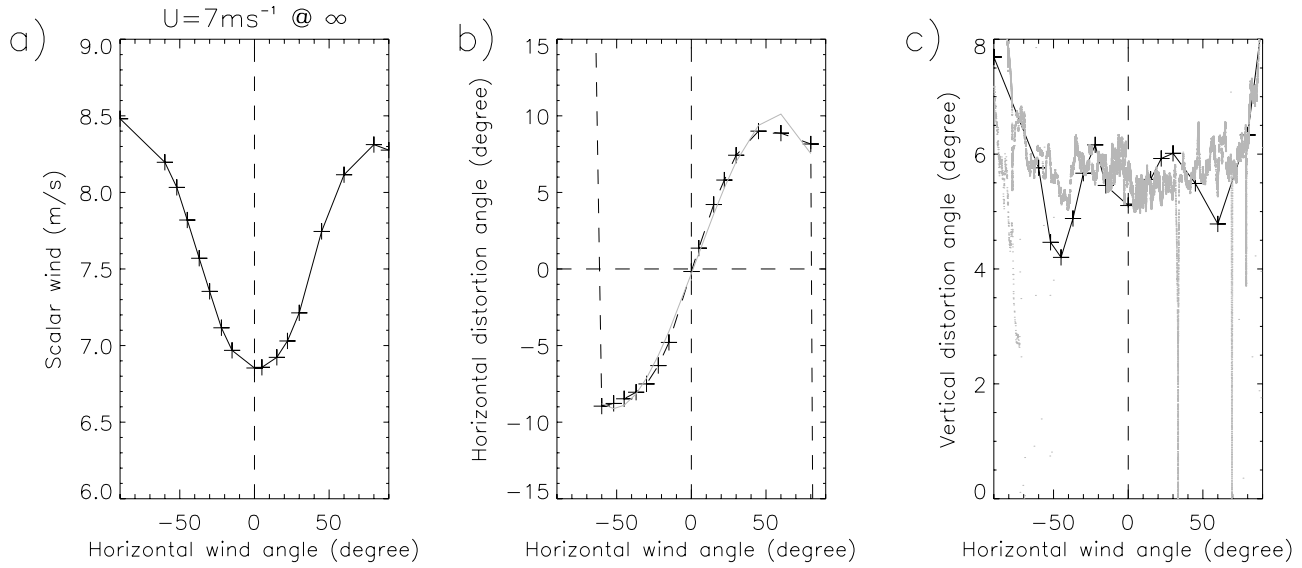

Figure 5. (a, b, c) Flow distortion effect from simulations and sonic anemometry.

Simulations and observations both reveal the asymmetry of the body of the ship, and the decrease in vertical wind angle at ±45° of azimuth wind angle. Part of the discrepancy visible in Figure 5c is possibly related to the accuracy with which the mast was modeled, which was limited for reasons of computer memory and CPU time consumption; but, the distortion simulation outlines the domain of validity for the measurement and gives typical orders of size. In the following, data corresponding to azimuth wind angles smaller than +35° only were selected. They correspond to real azimuth angles smaller than ±30°, to vertical wind angles in the range 5–6° and to a wind decrease smaller than 0.2 m s^{-1}. After a number of attempts, it was decided to apply only a 5.9° correction to the vertical angle, which is consistent with earlier studies [e.g., *Weill et al.*, 2003].

[17] In a second step, the design of the instrument mount was optimized. It was stressed that the height of the instruments could not be larger than 2 m above the platform so that maintenance was possible in cruise, and so as to avoid structural and vibration problems. The BEI motion pack was also sited as close as possible to the wind and humidity sensors, so that the wind correction could be applied without any distance correction for eddy correlation measurements. In previous experiments, the sensors were mounted on a sheet of metal (Figure 6), which served as a basis for new design improvements. With a flow inclined with a 15° vertical angle, the simulations revealed that sheet behaved like an aircraft wing, causing strong disturbances at the level of the refractometer and the Licor. In the final design, presented in Figure 1, the sheet was replaced with a tubular

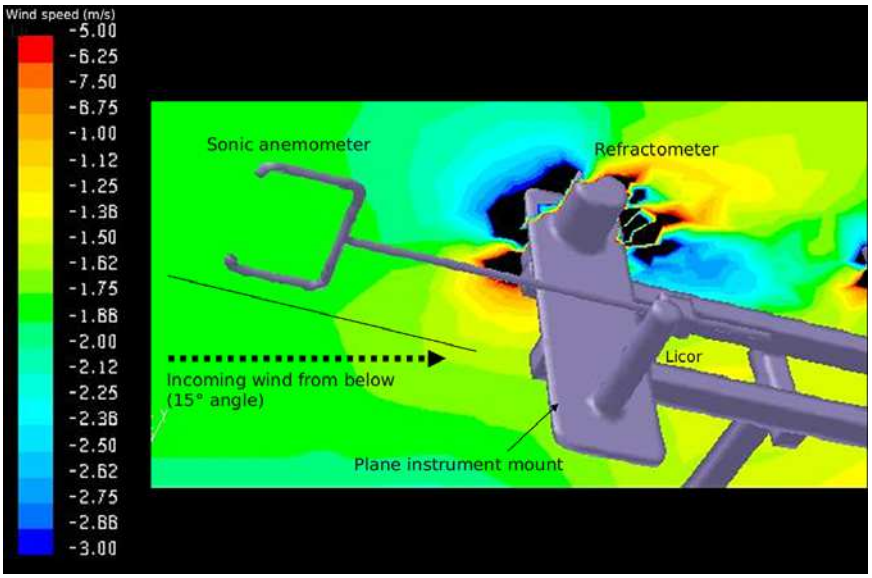

Figure 6. Contours of vertical flow angle for an incoming flow angle of 15° at infinite. The plane instrument mount acts like an aircraft wing. Its effect is to bend the flow and produce turbulence at the air intakes of the humidity sensors.

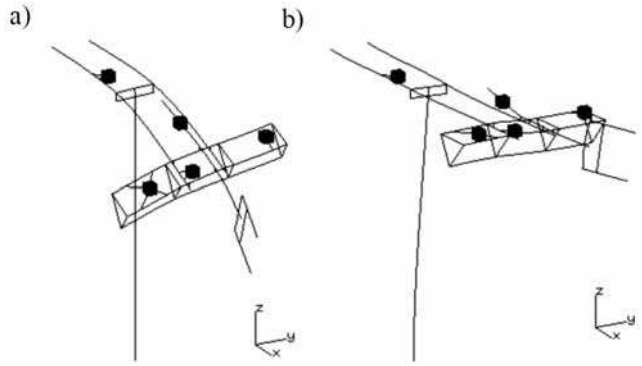

Figure 7. Main vibration modes of the flux instrument mount, below 25 Hz: (a) flexion of the horizontal mast and (b) flexion of the vertical mast.

structure, which is aerodynamically transparent. The sonic anemometer was placed 50 cm upstream the humidity sensors and the BEI. Humidity sensors were placed on each side, separated by 50 cm.

2.4. Modal Analysis

[18] For the calculation of turbulent quantities, it is critical that vibrations of the sensors be minimized. Although it is not intended to damp all vibrations which can affect a ship-based sensor, such as wave action, engine, and wind vibration, the platform design was refined to ensure there were no eigen modes below 25 Hz.

[19] Vibration simulations were performed at DT-INSU with the commercial software IDEAS (trademark). The analysis revealed two principal modes below 25 Hz (presented in Figure 7) that were the vertical swing of the horizontal mast at 20 Hz and the horizontal swing of the vertical mast at 23 Hz. In order to improve the design and reject these modes to higher frequencies, several configurations were tested, with additional structural support, or stabilizing cables. The best compromise in terms of aerodynamics, weight, performance and ease of installation was to add four cables (visible in Figure 1). With this configuration, the modes we rejected at 26.8 Hz and 53 Hz, respectively, which fulfils the initial requirements. Note however these results do not ensure that any vibrations below 26.8 Hz are removed from consideration. They instead signify that the tubular structure will not resonate at those frequencies.

3. Flux Calculation Methodology

[20] Two methods were used for estimating turbulent fluxes: (1) the eddy correlation method and (2) the inertial dissipation method.

3.1. Eddy Correlation Method

[21] The EC method is a direct application of the turbulent flux definition, which is written as,

$$\frac{\tau}{\rho} = \left(\overline{u'w'}^2 + \overline{v'w'}^2\right)^{1/2}, \tag{1}$$

$$\frac{H_S}{\rho C_p} = -\overline{\theta' w'}, \tag{2}$$

$$\frac{L_E}{\rho L_V} = -\overline{q' w'}, \tag{3}$$

where τ is the stress; H_S is the sensible heat flux; L_E is the Latent Heat flux; ρ is air density; C_p the specific heat of air; L_v is latent heat of vaporization of water; u, v, w are streamwise, crosswise, and upward wind components, respectively; θ is potential temperature; and q is specific humidity. Overbars denote averaging, whereas quantities with a quote denote turbulent fluctuations (quantity minus its average).

[22] A typical calculation of the EC momentum flux is based on a 22-min-long time series of wind components. After wind data are corrected for ship motion and flow distortion, and after removal of the linear trends, the covariance products "u times v" and "u times w" are calculated, and the results are averaged. Next the stress is calculated with (1).

[23] Careful correction of ship motion is essential for applying the EC method. The speed at which the ship translates or rotates contaminates wind speed measurements, which are given relative to the ship reference frame. The correction matrix described by *Edson et al.* [1998] apparently solves the problem, as it accounts for six degrees of freedom (three translations and three rotations) as well as the distance between accelerometers and the wind instrument. Unlike *Pedreros et al.* [2003] who recently applied the correction matrix in the context of the FETCH experiment, we were unsuccessful at using it for EGEE. The reason was that wind and ship velocities did not exactly match in time and amplitude. The time lag between ship and wind velocities ranged from 0.1 to 0.6 s, as shown in Figure 8. The technique used to find the time lag was to shift by an amount t_0 the time series of vertical wind, with respect to the vertical speed of the ship. The shifted vertical wind was then correlated to vertical ship motion. A large range of t_0 (-2 s to 2 s) was tested, until the best anticorrelation was found (vertical wind is directed downward when the ship goes up). Data were not used if anticorrelation was larger than -0.7. When converted to a distance, the time lag calculated ranged from 0 to 6 m (Figure 9), which clearly shows that the lag is not only related to the distance between wind and motion sensors, 0.5 m, as initially thought. It was also checked that the lag was not related to time synchronization problems between electronic signals, such as computer clock drift issues or times of message transmission between serial lines.

[24] A reasonable hypothesis is that time lag is related to flow distortion at turbulent scales. For example, when the ships takes a negative pitch angle, vertical wind velocity starts to decrease only a few instants after the ship bow as started to plunge. It is also important to note that only part of this negative ship velocity translates into a positive wind velocity (Figure 10). If one interprets the time lag and amplitude difference as flow distortion effects, then Figures 8 and 10 just reveal the amplitude and phase of the turbulent aerodynamic transfer function of the ship. With this context, a specific correction technique was set up for correcting wind data. Time series of vertical velocity were all shifted in time and multiplied by the amplitude

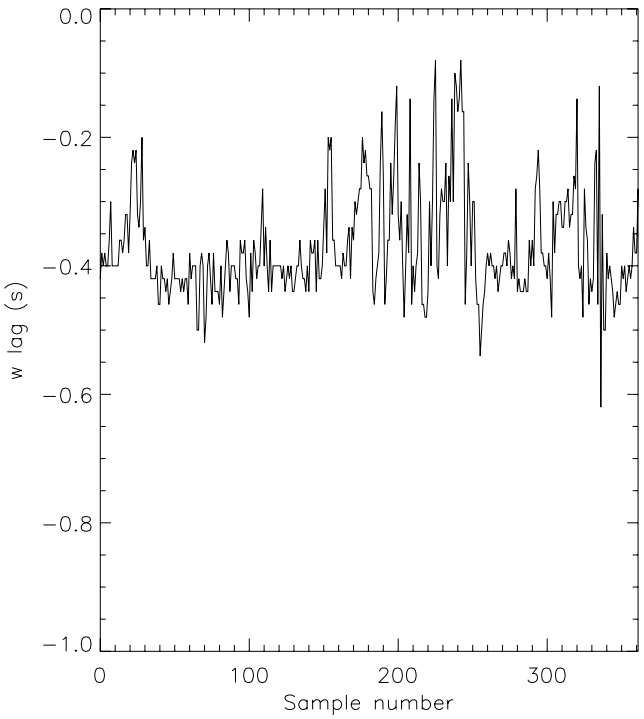

Figure 8. Time lag that corresponds to the maximum of correlation between vertical wind (w) and vertical ship velocity.

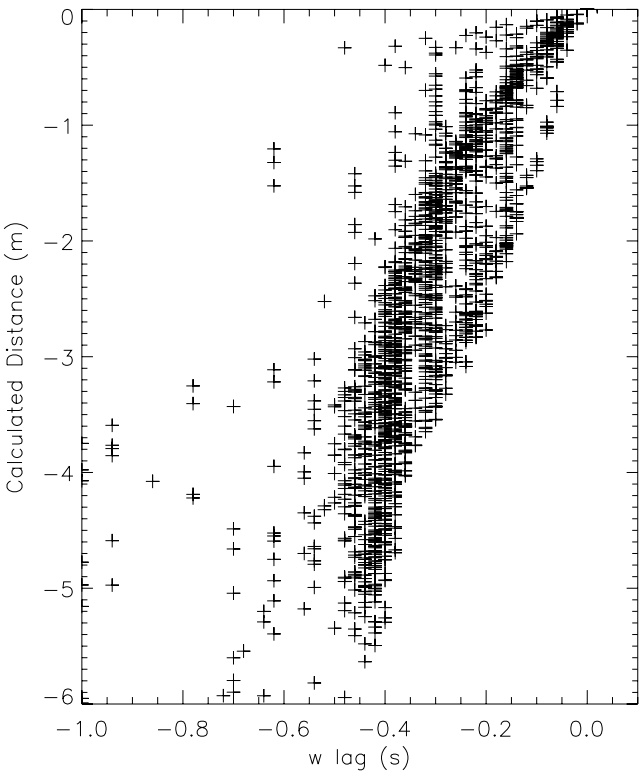

Figure 9. Distance that corresponds to the time lag as a function of vertical wind.

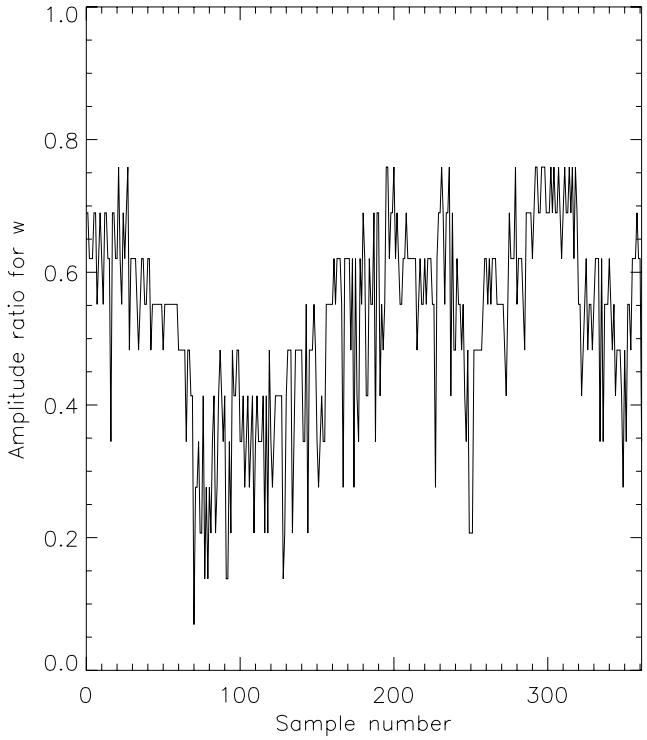

Figure 10. Amplitude ratio that minimizes the standard deviation between vertical wind and vertical ship velocity.

factors presented in Figures 8 and 10. Next, the corrected ship velocity was added to the wind velocity to produce corrected wind velocities.

3.2. Inertial Dissipation Method

[25] Unlike the EC method, which is based on the turbulent production zone of the wind power spectrum (from 22 min to 1 Hz), the ID method is based on the inertial zone of the spectrum (1–20 Hz), which is above the frequency of most ship motion. The application of the ID method consists in computing spectra of along-wind component (u). Next, the spectra are related to the rate of dissipation (ε) of turbulent kinetic energy (TKE), via the Kolmogorov relationship,

$$S(f) = c\varepsilon^{\frac{2}{3}}\left(\frac{2\pi}{\overline{U}}\right)^{-\frac{2}{3}} f^{-\frac{5}{3}} \tag{4}$$

where c is the Kolmogorov constant (0.55), U is the mean scalar relative wind, f is the frequency and S(f) is the energy spectral density of u. According to the TKE conservation equation, ε is related to the friction velocity (or u_*, the square of it is the opposite of the momentum flux), and the Monin-Obukhov dimensionless ratio ($z\,L^{-1}$) that defines air stability, which is written as,

$$0 = -\frac{z}{L} + \Phi\left(\frac{z}{L}\right) - \kappa\frac{z}{u_*^3}\left(\frac{1}{\rho}\frac{\partial}{\partial z}\left(\overline{w'p'}\right) - \frac{\partial}{\partial z}\left(\overline{w'e}\right)\right) - \kappa\frac{z}{u_*^3}\varepsilon \tag{5}$$

where κ is the Von Karman constant and Φ is the wind gradient similarity function. Advection and time derivative

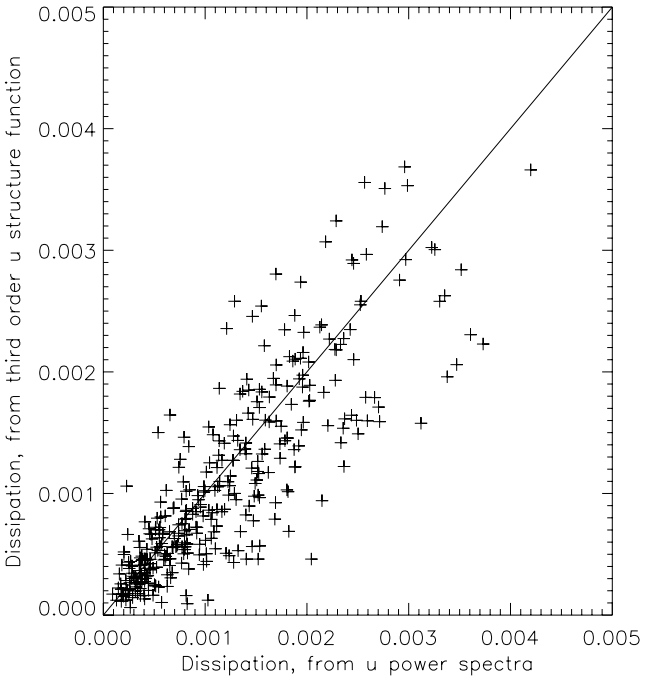

Figure 11. Dissipation rate calculated with two methods: third-order structure function (y axis) and power spectra of along-wind component (x axis).

terms were neglected in equation (5). The third r.h.s. term is the vertical divergence of the correlation between pressure fluctuation and vertical velocity minus the vertical divergence of the correlation between vertical velocity fluctuations and turbulent kinetic energy. The sum of the pressure plus TKE diffusion terms in (5) is often referred to as ''imbalance term'' in the literature [*Taylor and Yelland*, 2000; *Dupuis et al.*, 1997]. According to *Dupuis et al.* [1997], the imbalance term should be parameterized as a function of z L^{-1}, whereas *Taylor and Yelland* [2000] assume that the imbalance term is nothing but a noise. Other authors (see a review by *Högström* [1996]) also question the correct value of the Kolmogorov constant (c) that is used in the ID method. In the present study, the validity of both hypotheses was checked with the method described hereafter.

[26] In the Kolmogorov theory, the relationship between the third-order wind structure function and ε is exact,

$$\overline{(u(l+dl)-u(l))^3} = -\frac{4}{5}\varepsilon dl \tag{6}$$

where l is a distance and dl is a distance increment. With the frozen turbulence hypothesis available for small time increments (equivalent to spatial increments in the inertial subrange), a time structure function is immediately derived,

$$\overline{(u(t+dt)-u(t))^3} = -\frac{4}{5}\varepsilon U dt \tag{7}$$

[27] From equations (4) and (7), two methods are now available for calculating the turbulent dissipation rate, referred to as ε_5 and ε_8, respectively hereafter. The comparison between ε_5 and ε_8 is shown in Figure 11. The correlation is 0.85 and the RMS deviation is 0.4×10^{-3}, which indicates a reasonable scatter, given that the third power of wind increment is taken in equation (7). From equations (4) and (7), a measure of the Kolmogorov constant can be obtained,

$$c = 0.55\left(\frac{\varepsilon_5}{\varepsilon_8}\right)^{\frac{2}{3}} \tag{8}$$

[28] According to EGEE data, c is 0.63. This value of c is 14% larger than the commonly accepted value of 0.55, which is significantly overestimated, but consistent. According to this only result, it is not clear whether the value of c should be changed, or an imbalance term should be used (or both) in the ID method. To answer this question, ID friction velocities calculated with several values of c and the imbalance term were compared to bulk friction velocities (on the basis of the parameterization of the drag coefficient by *Smith* [1980]). The parameter c was taken to be equal to 0.55 or to 0.63, while 100 values of the imbalance term were selected between -2 z L^{-1} and 2 z L^{-1} by step of 0.0025 z L^{-1}. Next, the value of the imbalance term for which the comparison between ID and bulk u* was best in terms of correlation and root mean square deviation was determined. As shown in Figure 12, agreement was obtained with c equal to 0.55 and the imbalance term equal to -0.46 z L^{-1}. This result is consistent with the findings of *Dupuis et al.* [1997] during the SOFIA/ASTEX experiment, an experiment with calm sea conditions, like EGEE. Therefore, the results presented above show that the comparison between ID and bulk friction velocities are significantly improved when the imbalance term is accounted for, and not when c is modified. Subsequently, the value of 0.63 found for c with equation (7) is not exact. The estimated value of c possibly differs from 0.55 because of measurement uncertainties, and because not all of the hypotheses made, such as frozen turbulence, local isotropy, and homogeneity were fully valid.

4. Fluxes and Exchange Coefficients

4.1. Comparison Between ID and EC Fluxes

[29] Friction velocities calculated with the ID and EC methods agree well as shown in Figure 13. The correlation coefficient is 0.84 and the RMS deviation between ID and EC methods for u_* is 0.033 which is 8–30% at 0.1–0.4 m s^{-1}. The systematic deviation between ID u_* and EC u_* is negligible.

[30] Sensible and latent heat fluxes calculated with ID and EC methods are referred to as HSID, HSEC, LEID, and LEEC hereafter. The RMS deviation found between HSEC and HSID is small, 3.82 W m^{-2} (Figure 14). The systematic deviation between HSEC and HSID is also small, on the order of 2 W m^{-2}, but Figure 14 reveals that large HSID values are overestimated compared to HSEC.

[31] The RMS deviation between LEEC and LEID is slightly smaller with the refractometer (20 W m^{-2}), than with the Licor (24 W m^{-2}), as shown in Figure 15. As shown in Figure 15, the bias is apparently better controlled with the refractometer (18 W m^{-2}) than with the Licor (33 W m^{-2}).

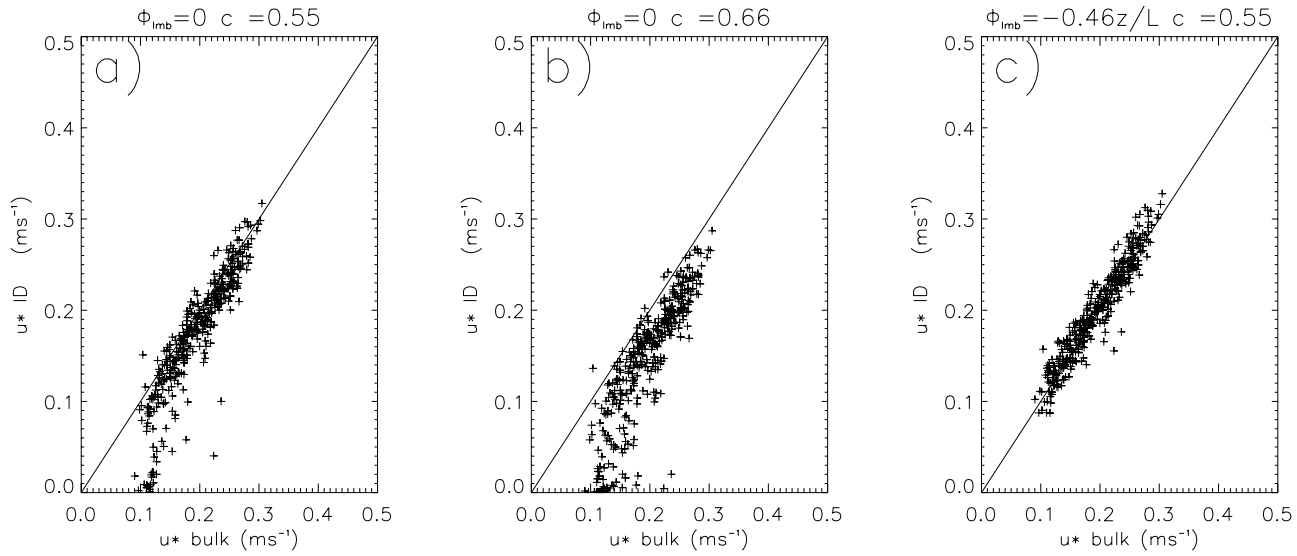

Figure 12. Comparison between bulk u* and ID u*. (a, b, c) The ID method was successively applied with different values of Φ_{imb} and c (Kolmogorov constant).

However, the values of the biases are large, and are difficult to explain. Independent comparisons of EC and ID flux estimates to bulk flux estimates were performed, and gave the following results. Refractometer LEID values are slightly underestimated with respect to bulk estimates, by 7 W m^{-2}, whereas the bias between LEEC and bulk flux estimates is −40 W m^{-2}. This strongly suggests that the −33 W m^{-2} bias is mostly related to the application of the EC method. Problems with ship motion correction and/or a lack of coherence between times series of humidity and corrected wind possibly explain this large bias. The lack of coherence could arise from local flow distortion, possibly related to the location of the mast that is not enough close to the bow, or a problem in the data processing, but it is not clearly explained so far.

4.2. Exchange Coefficients

[32] The calculation of exchange coefficients was done with EC and ID methods. The drag coefficients are similar at winds larger than 7 m s^{-1}, and are consistent with *Smith* [1980], as shown in Figure 16. Below 7 m s^{-1}, the scatter is larger. The EC drag coefficients increase as wind decreases, as opposed to the ID drag coefficient, which is almost constant and is consistent with *Smith* [1980], though over-

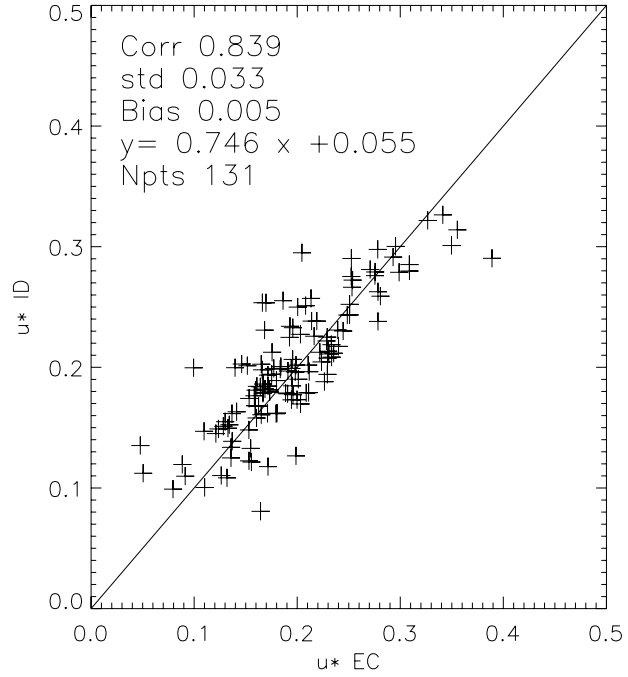

Figure 13. Comparison of EC and ID friction velocities.

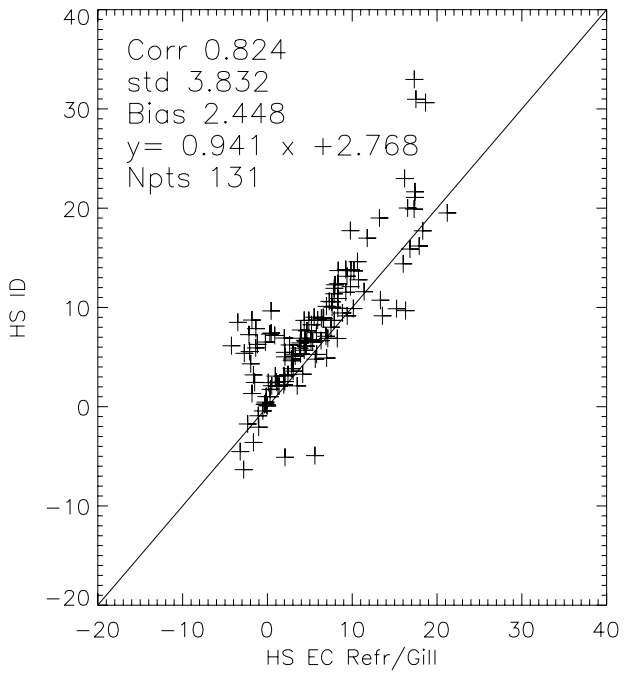

Figure 14. Comparison of EC and ID sensible heat fluxes.

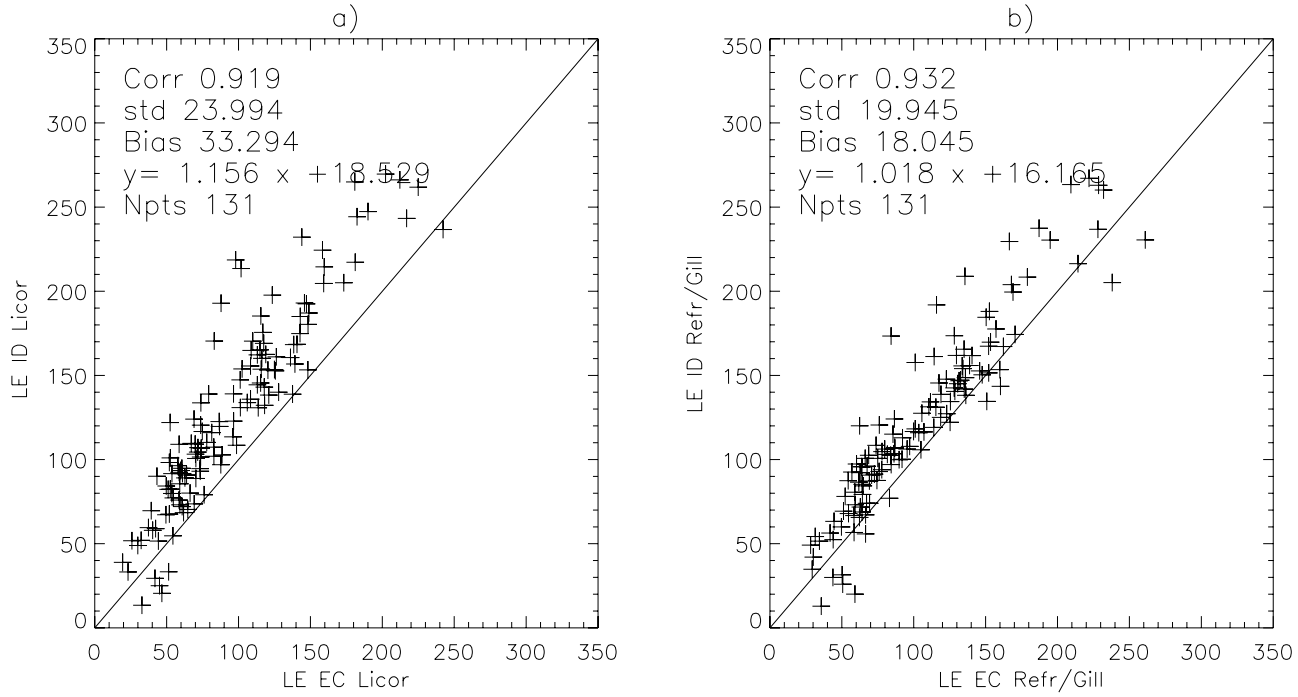

Figure 15. Comparison of EC and ID latent heat fluxes. (a) Data from the Licor and (b) refractometer data.

estimated by 0.2 10^{-3}. Confidence in the ID drag coefficient is better than in the EC coefficient, because the scatter is smaller, as shown in Figure 16. Therefore, EGEE data indicate that CD is 1.1 $\times$ 10^{-3} below 7 m s^{-1}. Note the exchange coefficients calculated with the ID method were tuned to bulk estimates, as described in section 3.2. Consequently, ID and bulk coefficients are not totally independent, specifically at friction velocities smaller than 0.15 m s^{-1} (this threshold was inferred from data presented in Figure 3).

[33] CH values calculated with the ID method agree well with *DeCosmo et al.* [1996] at winds larger than 5.5 m s^{-1} (Figure 17). However, CH values are overestimated with respect to *Smith* [1980], below 5.5 m s^{-1}. The coefficients calculated with ID and EC methods are consistent. However, the scatter is large below 5.5 m s^{-1} so that it is difficult to draw firm conclusions on the increase of CH at low wind speeds. Figure 17 also reveals that EC CH is underestimated by a factor ~2 with respect to ID CH and the *DeCosmo et al.*

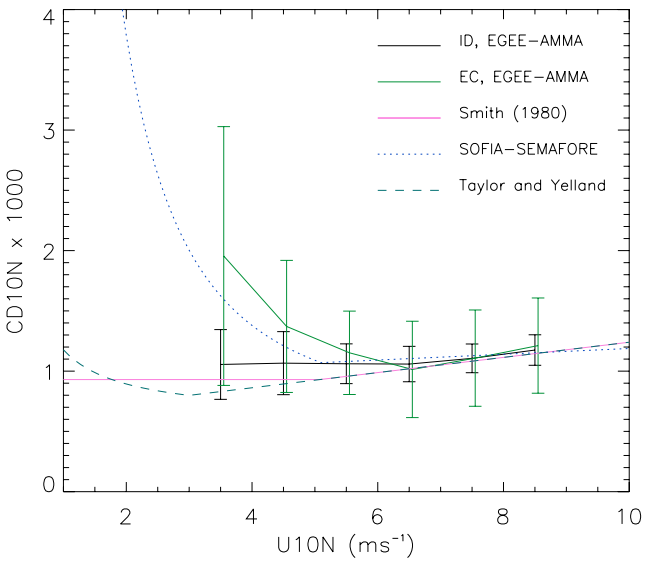

Figure 16. Neutral 10 m drag coefficient as a function of 10 m neutral wind. The vertical bars denote the standard deviation of CD10N.

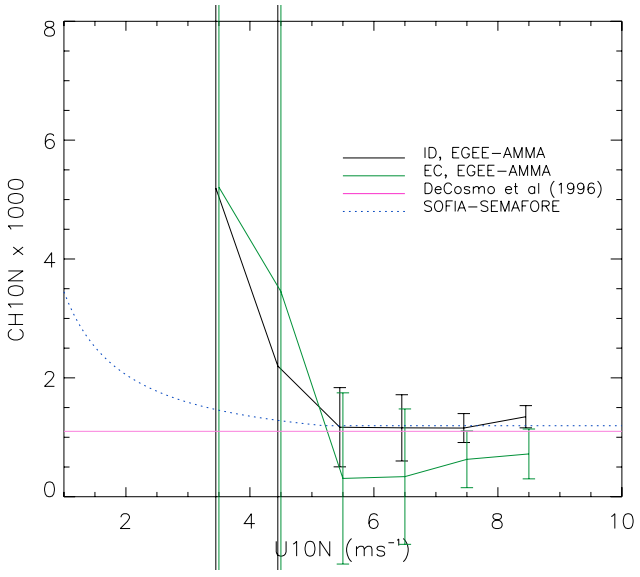

Figure 17. Neutral 10 m Stanton number as a function of 10 m neutral wind. The vertical bars denote the standard deviation of CH10N.

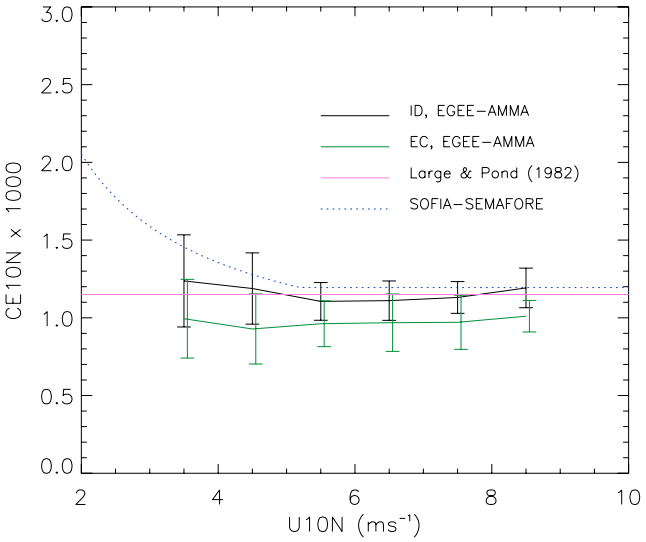

Figure 18. Neutral 10 m Dalton number as a function of 10 m neutral wind. The vertical bars denote the standard deviation of CE10N.

[1996] coefficients. The factor 2 seems unrealistic and rather suggests a systematic deviation of HSEC estimates.

[34] The systematic deviation between ID CE and EC CE is 0.2 10^{-3}, which is large. As for CH, there is a better agreement between ID CE and *DeCosmo et al.* [1996] than EC CE and *DeCosmo et al.* [1996]. In spite of the discrepancies between coefficients in terms of systematic deviation, as shown in Figure 18, the relationship between CE and the neutral wind is consistent with the ID and EC methods. Indeed, CE slightly increases if wind is larger than 7 m s^{-1} or if it is smaller than 5 m s^{-1}. The best fit between ID data and neutral wind is written as,

$$CE_{10N} = 0.017 \times U_{10N}^2 - 0.22 \times U_{10N} + 1.8, \qquad (9)$$

which corresponds to CE_{10N} values smaller than *Dupuis et al.'s* [1997] and larger than *Large and Pond's* [1982] at winds smaller than 5 m s^{-1}.

5. Conclusion

[35] Several observations can be drawn from EGEE experiment.

[36] 1. From a technical point of view, the new turbulent package and installation on board the R/V *Atalante* have been determined to be a significant improvement on the design used during the FETCH experiment mainly because of the precise characterization and remediation of flow distortion and vibration.

[37] 2. Fluxes have been estimated using ID and EC methods, and the differences between fluxes as estimated by the two methods have been found to be relatively small especially for friction velocity (no bias and a small standard deviation of 0.03 m s^{-1}). Calculated sensible heat fluxes are reasonably comparable with a small bias and an acceptable scatter, 2.4 W m^{-2} and 3.8 W m^{-2}, respectively; latent heat fluxes, though well correlated and with a low scatter, present a large bias of ~33 W m^{-2} using the Licor and 18 W m^{-2} with the refractometer, but with a comparable scatter close to 20 W m^{-2}.

[38] 3. In the ID method we have computed the turbulent dissipation rate using the second-order (spectral density) and the third-order temporal structure functions. The two estimates have compared favorably, and the incidence of the estimates on the Kolmogorov constant and the imbalance parameterization was studied. A statistical analysis of the impact on the measurement of the Kolmogorov constant choice and the use of the *Dupuis et al.* [1997] imbalance parameterization is in favor of the imbalance parameterization in calm sea conditions such as occurred in EGEE and SEMAPHORE. This result suggests that the next step is to directly measure the imbalance term, both in calm conditions and in a range of sea states (D. Bourras et al., Static pressure fluctuations derived from a new type of probe, submitted to *Journal of Geophysical Research*, 2009).

[39] 4. We observe that flux parameterizations do not differ considerably from previous experiments, and for low U_{10N} (<4 m s^{-1}), their validity remain always questioning. The parameterizations found are however in the uncertainty range of parameterizations found in the literature.

[40] **Acknowledgments.** On the basis of French initiative, AMMA was built by an international scientific group and is currently funded by a large number of agencies, especially from France, United Kingdom, United States, and Africa. It has been the beneficiary of a major financial contribution from the European Community's Sixth Framework Research Programme. Detailed information on scientific coordination and funding is available on the AMMA International web site (http://www.amma-international.org).

References

Bourlès, B. (2003), On the Gulf of Guinea and the West African Monsoon, *CLIVAR Exch. Lett.*, *27*(8), 2–3.

Bourlès, B., P. Brandt, G. Caniaux, M. Dengler, Y. Gouriou, E. Key, R. Lumpkin, F. Marin, R. L. Molinari, and C. Schmid (2007), African Monsoon Multidisciplinary Analysis (AMMA): Special measurements in the tropical Atlantic, *CLIVAR Exch.*, *41*(2), 7–9.

Bourlès, B., et al. (2008), The PIRATA program: History, accomplishments and future directions, *Bull. Am. Meteorol. Soc.*, *89*, 1111–1125, doi/10.1175/2008BAMS2462.1..

Bourras, D. (2006), Comparison of five satellite derived latent heat flux products to moored buoy data, *J. Clim.*, *19*, 6291–6313, doi:10.1175/JCLI3977.1.

Bradley, E. F., P. A. Coppin, and J. S. Godfrey (1991), Measurements of sensible and latent heat fluxes in the western equatorial Pacific Ocean, *J. Geophys. Res.*, *96*, 3375–3389.

Brut, A., A. Butet, P. Durand, G. Caniaux, and S. Planton (2005), Air-sea exchanges in the equatorial area from the EQUALANT99 dataset: Bulk parametrizations of turbulent fluxes corrected for airflow distortion, *Q. J. R. Meteorol. Soc.*, *131*, 2497–2538, doi:10.1256/qj.03.185.

Caniaux, G., A. Brut, D. Bourras, H. Giordani, A. Paci, L. Prieur, and G. Reverdin (2005), A 1 year sea surface heat budget in the northeastern Atlantic basin during the POMME experiment: 1. Flux estimates, *J. Geophys. Res.*, *110*, C07S02, doi:10.1029/2004JC002596.

Champagne, F., C. Friehe, J. LaRue, and J. Wynagaard (1977), Flux measurements, flux estimation techniques, and fine-scale turbulence measurements in the unstable surface layer over land, *J. Atmos. Sci.*, *34*, 515–530, doi:10.1175/1520-0469(1977)034<0515:FMFETA>2.0.CO;2.

Dardier, G., A. Weill, H. Dupuis, C. Guerin, W. M. Drennan, S. Brachet, F. Lohou, and R. Pedreros (2003), Constraining the inertial dissipation method using the vertical velocity variance, *J. Geophys. Res.*, *108*(C3), 8063, doi:10.1029/2002JC001667.

DeCosmo, J., K. B. Katsaros, S. D. Smith, R. J. Anderson, W. A. Oost, K. Bumke, and H. Chadwick (1996), Air-sea exchange of water vapor and sensible heat: The Humidity Exchange over Sea (HEXOS) results, *J. Geophys. Res.*, *101*, 12,001–12,016, doi:10.1029/95JC03796.

Delahaye, J. Y., C. Guerin, J. P. Vinson, H. Dupuis, A. Weill, H. Branger, L. Eymard, J. Lavergnat, and G. Lachaud (2001), A new shipborne microwave refractometer for estimating the evaporation flux at the sea surface, *J. Atmos. Oceanic Technol.*, *18*, 459–475, doi:10.1175/1520-0426(2001)018<0459:ANSMRF>2.0.CO;2.

Drennan, W., M. Donelan, E. Terray, and K. Katsaros (1996), Oceanic turbulence dissipation measurements in SWADE, *J. Phys. Oceanogr.*, *26*, 808–815, doi:10.1175/1520-0485(1996)026<0808:OTDMIS>2.0.CO;2.

Dupuis, H., A. Weill, K. B. Katsaros, and P. K. Taylor (1995), Turbulent heat fluxes by profile and inertial dissipation methods: Analysis of the atmospheric surface layer from shipboard measurements during the SOFIA/ASTEX and SEMAPHORE experiments, *Ann. Geophys.*, *13*, 1065–1074, doi:10.1007/s00585-995-1065-0.

Dupuis, H., P. K. Taylor, A. Weill, and K. B. Katsaros (1997), The inertial dissipation method applied to derive momentum fluxes over the ocean during the SOFIA/ASTEX and SEMAPHORE experiments with low to moderate wind speeds, *J. Geophys. Res.*, *102*, 21,115–21,129, doi:10.1029/97JC00446.

Dupuis, H., C. Guerin, D. Hauser, A. Weill, P. Nacass, W. Drennan, S. Cloché, and H. Graber (2003), Impact of flow distortion corrections on turbulent fluxes estimated by the inertial dissipation method during the FETCH experiment on R/V *L'Atalante*, *J. Geophys. Res.*, *108*(C3), 8064, doi:10.1029/2001JC001075.

Edson, J. B., C. W. Fairall, S. E. Larsen, and P. G. Mestayer (1991), A study of the inertial-dissipation technique for computing air-sea fluxes, *J. Geophys. Res.*, *96*, 10,689–10,711, doi:10.1029/91JC00886.

Edson, J. B., J. E. Hare, and C. W. Fairall (1998), Direct covariance flux estimates from moving platforms at sea, *J. Atmos. Oceanic Technol.*, *15*, 547–562, doi:10.1175/1520-0426(1998)015<0547:DCFEFM>2.0.CO;2.

Eymard, L., et al. (1999), Surface fluxes in the North Atlantic current during the CATCH/FASTEX experiment, *Q. J. R. Meteorol. Soc.*, *125*, 3563–3599, doi:10.1002/qj.49712556121.

Eymard, L., A. Weill, D. Bourras, C. Guérin, P. Le Borgne, and J. M. Lefèvre (2003), Use of ship mean data for validating model and satellite flux fields during the FETCH experiment, *J. Geophys. Res.*, *108*(C3), 8060, doi:10.1029/2001JC001207.

Fairall, C. W., E. F. Bradley, D. P. Rogers, J. B. Edson, and G. S. Young (1996), Bulk parameterization of air-sea fluxes in TOGA COARE, *J. Geophys. Res.*, *101*, 3747–3767.

Fairall, C. W., A. B. White, J. B. Edson, and J. E. Hare (1997), Integrated shipboard measurements of the marine boundary layer, *J. Atmos. Oceanic Technol.*, *14*, 338–359, doi:10.1175/1520-0426(1997)014<0338:ISMOTM>2.0.CO;2.

Hauser, D., et al. (2003), The FETCH experiment: An overview, *J. Geophys. Res.*, *108*(C3), 8053, doi:10.1029/2001JC001202.

Högström, U. (1996), Review of some basic characteristics of the atmospheric surface layer, *Boundary Layer Meteorol.*, *78*, 215–246, doi:10.1007/BF00120937.

Kolmogorov, A. N. (1941), Dissipation of energy in locally isotropic turbulence, *Dokl. Akad. Nauk*, *32*, 16–18.

Large, W. G., and S. Pond (1982), Sensible and latent heat fluxes over the ocean, *J. Phys. Oceanogr.*, *12*, 464–482, doi:10.1175/1520-0485(1982)012<0464:SALHFM>2.0.CO;2.

Monin, A. S., and A. M. Obukhov (1954), Basic laws of turbulent mixing in the surface layer of the atmosphere, *Trudy Geofiz. Inst. Akad. Nauk. SSR*, *24*, 1–24.

Pedreros, R., G. Dardier, H. Dupuis, H. C. Graber, W. M. Drennan, A. Weill, C. Guérin, and P. Nacass (2003), Momentum and heat fluxes via the eddy correlation method on the R/V *L'Atalante* and an ASIS buoy, *J. Geophys. Res.*, *108*(C11), 3339, doi:10.1029/2002JC001449.

Persson, P. O. G., J. E. Hare, C. W. Fairall, and W. D. Otto (2005), Air-sea interaction processes in warm and cold sectors of extratropical cyclonic storms observed during FASTEX, *Q. J. R. Meteorol. Soc.*, *131*, 877–912.

Redelsperger, J. L., C. Thorncroft, A. Diedhiou, T. Lebel, D. J. Parker, and J. Polcher (2006), African Monsoon Multidisciplinary Analysis (AMMA): An International Research Project and Field Campaign, *Bull. Am. Meteorol. Soc.*, *87*, 1739–1746.

Servain, J., A. J. Busalacchi, M. J. McPhaden, A. D. Moura, G. Reverdin, M. Vianna, and S. E. Zebiak (1998), A Pilot Research Moored Array in the Tropical Atlantic (PIRATA), *Bull. Am. Meteorol. Soc.*, *79*, 2019–2031, doi:10.1175/1520-0477(1998)079<2019:APRMAI>2.0.CO;2.

Smith, S. D. (1980), Wind stress and heat flux over the ocean in gale force winds, *J. Phys. Oceanogr.*, *10*, 709–726, doi:10.1175/1520-0485(1980)010<0709:WSAHFO>2.0.CO;2.

Taylor, P. K., and M. J. Yelland (2000), A note on the apparent "imbalance" term in the Turbulent Kinetic Energy Budget, *J. Atmos. Oceanic Technol.*, *17*, 82–89, doi:10.1175/1520-0426(2000)017<0082:OTAITI>2.0.CO;2.

Traullé, O., et al. (2008), Mesures météorologiques réalisées sur le N/O L'*Atalante* pendant la campagne AMMA/EGEE3. Acquisition-Traitement-Validation (in French), technical note, Cent. Natl. de Rech. Météorol. Groupe de Météorol. Exp. et Instrum., Toulouse, France, 121 pp.

Weill, A., et al. (1995), SOFIA 1992 experiment during ASTEX, *Global Atmos. and Ocean Syst.*, *3*, 355–395.

Weill, A., et al. (2003), Toward a better determination of turbulent air-sea fluxes from several experiments, *J. Clim.*, *16*, 600–618, doi:10.1175/1520-0442(2003)016<0600:TABDOT>2.0.CO;2.

Yelland, M. J., B. I. Moat, P. K. Taylor, R. W. Pascal, J. Hutchings, and V. C. Cornell (1998), Wind stress measurements from the open ocean corrected for air flow distortion by the ship, *J. Phys. Oceanogr.*, *28*, 1511–1526, doi:10.1175/1520-0485(1998)028<1511:WSMFTO>2.0.CO;2.

Yelland, M. J., B. I. Moat, R. W. Pascal, and D. I. Berry (2002), CFD model estimates of the airflow distortion over research ships and the impact on momentum flux measurements, *J. Atmos. Oceanic Technol.*, *19*, 1477–1499, doi:10.1175/1520-0426(2002)019<1477:CMEOTA>2.0.CO;2.

J. Barrié, G. Bouhours, G. Caniaux, D. Legain, B. Piguet, and O. Traullé, GAME, CNRM, Météo-France, 42 Avenue Gaspard Coriolis, F-31057 Toulouse, France.

F. Baudin, C. Berthod, A. Clémençon, and S. Letourneur, DT, INSU, 1 Place Aristide Briand, F-92195 Meudon, France.

B. Bourlès, IRD, B.P. 70, F-29280 Plouzané, France.

D. Bourras, F. Boutet, J. P. Vinson, and A. Weill, CETP, 10-12 Avenue de l'Europe, F-78140 Vélizy-Villacoublay, France. (denis.bourras@cetp.ipsl.fr)

L. Eymard, LOCEAN, 4 Place Jussieu, F-75252 Paris, France.

E. Key, RSMAS, University of Miami, Miami, FL 33149-1098, USA.

B. Sinardet, Institut Carnot de Bourgogne, 6 Boulevard Gabriel, F-21000 Dijon, France.